Mon. Not. R. Astron. Soc. **000**, 1–?? (1998) Printed 1 February 2008 (MN LaTeX style file v1.4)

An empirical calibration of nebular abundances based on the sulphur emission lines.

Angeles I. Díaz and Enrique Pérez-Montero
Dpto. de Física Teórica, C-XI, Universidad Autónoma de Madrid, Cantoblanco, 28049-Madrid, Spain

Accepted . Received 1998

ABSTRACT

We present an empirical calibration of nebular abundances based on the strong emission lines of [SII] and [SIII] in the red part of the spectrum through the definition of a sulphur abundance parameter S_{23}. This calibration presents two important advantages against the commonly used one based on the optical oxygen lines: it remains single-valued up to abundances close to solar and is rather independent of the degree of ionization of the nebula.

Key words: Galaxies: abundances – nebulae: HII regions

1 INTRODUCTION

The analysis of nebular spectra constitutes the best, and in some cases the only one, method for the determination of chemical abundances in spiral and irregular galaxies, as well as in sites of recent star formation. The abundances of several elements like He, O, N and S can in principle be determined since strong emission lines of these elements, some of them in their dominant ionization states, are present in the optical region of the spectrum. This requires knowledge of the electron temperature which can be obtained by measuring appropriate line ratios like [OIII] $\frac{\lambda4363}{\lambda4959+\lambda5007}$, [NII] $\frac{\lambda5755}{\lambda6548+\lambda6584}$, [OII]$\frac{\lambda7327}{\lambda3727+\lambda3729}$, or [SIII]$\frac{\lambda6312}{\lambda9069+\lambda9532}$.

Unfortunately, these line ratios usually involve one intrisically weak line which can be detected and measured with confidence only for the brighter and hotter objects and in many cases – distant galaxies, low surface brightness objects, relatively low excitation regions – they become too faint to be observed.

In these cases, an empirical method based on the intensities of the easily observable optical lines is widely used. The method, originally proposed by Pagel *et al.* (1979) and Alloin *et al.* (1979), relies on the variation of these lines with oxygen abundance. Pagel *et al.* (1979) defined an abundance parameter $R_{23} = \frac{[OII]\lambda3727+[OIII]\lambda4959+\lambda5007}{H\beta}$ which increases with increasing abundance for abundances lower than about 20% solar, and then reverses its behavior, decreasing with increasing abundance, since above this value a higher oxygen abundance leads to a more effective cooling, the electron temperature gets lower and the optical emission lines get weaker.

In principle, the calibration of the R_{23} *versus* oxygen abundance relation can be done empirically in the low metallicity regime where electron temperatures can be derived directly, but requires the use of theoretical models for the so called high abundance branch. Several different calibrations have been made (Edmunds & Pagel 1984; McCall *et al.* 1985; Evans & Dopita 1986; Skillman 1989; McGaugh 1991) as more observational data and more improved models have become available. However, two problems that are difficult to solve still remain. The first one is related to the two-valued nature of the calibration, which can lead to important errors in the derived abundances. The second one concerns the dependence of R_{23} on the degree of ionization of the nebula (see Skillman 1989). R_{23} also depends on density, but this can be considered as a second order effect for low density regions ($n_H \simeq 100$ cm^{-3}) which constitute the majority of the extragalactic population. These two facts, taken together, produce a large dispersion of the data for values of $logR_{23} \geq 0.8$ and $12+log(O/H) \geq 8.0$, with objects with the same value of $logR_{23}$ having actual abundances which differ by almost an order of magnitude. Unfortunately, a significant number of objects (about 40% of the observed HII galaxies; Díaz 1999) have $logR_{23} \geq 0.8$ for which the calibration is most uncertain, and this percentage is even higher for HII regions in normal spiral galaxies.

Here we present an alternative abundance calibration based on the intensities of the sulphur lines: [SII] λ 6716, λ 6731 and [SIII] λ 9069, λ 9532, through the use of the sulphur abundance parameter S_{23} (Vílchez & Esteban 1996).

Spectroscopically, these lines are analogous to the optical oxygen lines defining R_{23} but, due to their longer wavelengths, their contribution to the cooling of the nebula should become important at a somewhat lower temperature. Yet, the lower abundance of sulphur makes these lines less significant than the [OIII] lines as a contributor to cooling. On the other hand, the sulphur lines are less sensitive to temperature, therefore the reversal in the relation between their

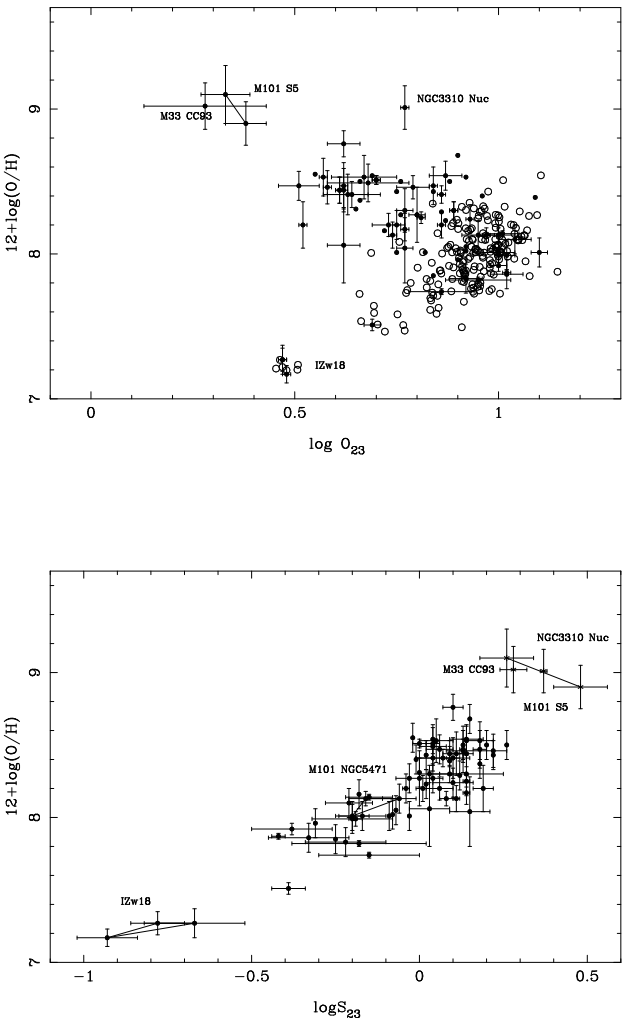

Figure 1. Oxygen abundance parameter (upper panel) and sulphur abundance parameter (lower panel) *vs* oxygen abundance for the objects in Table 2 and HII galaxies in Díaz (1998)

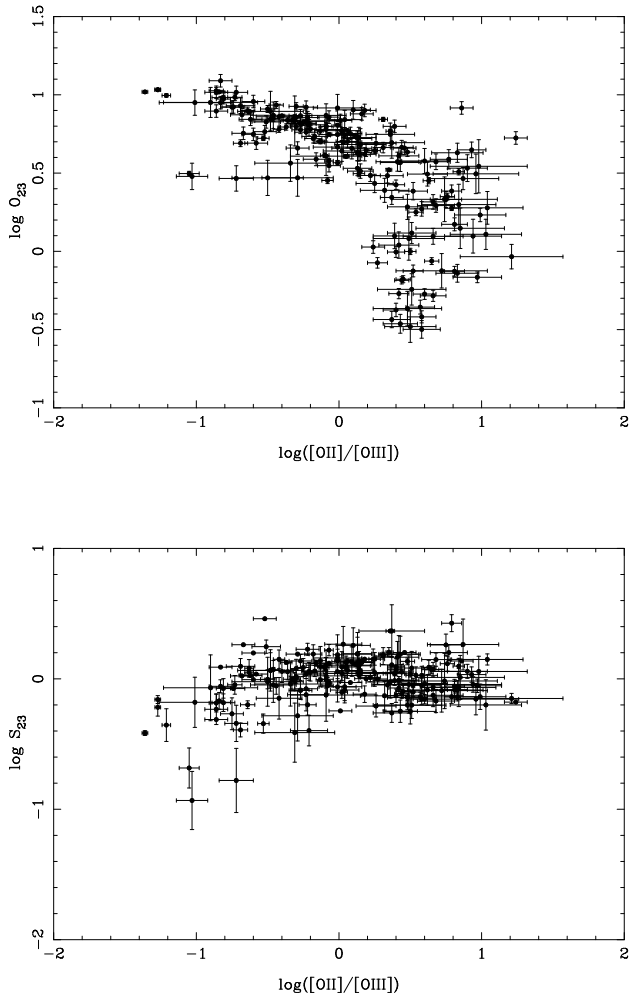

Figure 2. Relation between log_{O23} (upper panel) and $logS_{23}$ (lower panel with $log([OII]/[OIII])$, taken as ionization parameter indicator, for the objects in Table 1.

intensities and the average nebular abundance is expected to occur at a higher metallicity and the relation should remain single valued longer.

From the observational point of view they present two important advantages: first, the lines are easily detected both in high and low excitation ionized regions (Díaz *et al.* 1990) and second, they are less affected by reddening; moreover, they can be measured relative to nearby hydrogen recombination lines, Hα in the case of the [SII] lines and Paschen lines in the case of the [SIII] lines, which minimizes also any flux calibration uncertainties. These lines are accessible spectroscopically with CCD detectors up to a redshift of about 0.1.

2 OBSERVATIONAL DATA

In the last decade there has been a considerable increase in the amount of near infrared [SIII] emission line data. We have compiled from the literature all the HII region like objects for which measurements of these lines, together with optical emission lines exist. The sample includes HII regions in our own Galaxy, HII regions in spirals and irregular galaxies and HII galaxies. The data are presented in Table 1, where the logarithmic intensities of the emission lines with respect to Hβ are given, together with their corresponding observational errors when quoted in the original reference. These references are numbered in column 3 and listed at the bottom of the table. The observed intensities were corrected for reddening according to the derived logarithmic extinction at $H\beta$ listed in the last column of the table and a standard reddening law. The sample comprises a total of 196 objects.

Only 65 of these objects have electron temperatures derived directly. Table 2 lists for these objects their electron temperature, in units of 10^4 K, and their derived oxygen abundance expressed as $12 + log\frac{O}{H}$. The electron temperature has been derived from the measured intensity of the [OIII] λ 4363 line except for the objects marked with an as-

Table 1. Oxygen and Sulphur emission line intensities

Galaxy	**Region**	**Ref.**	**[OII]** 3727+ 3729	**Δ**	**[OIII]** 4959 + 5007	**Δ**	**[SII]** 6716+6731	**Δ**	**[SIII]** 9069+9532	**Δ**	**c(Hβ)**
MWG	NGC2467	1	0.49	—	0.41	—	-0.71	—	-0.13	—	0.60
–	ETACAR	1	0.19	—	0.48	—	-0.54	—	0.10	—	0.70
–	M17	1	0.05	—	0.65	—	-1.19	—	0.18	—	1.32
–	M16	1	0.21	—	0.28	—	-0.65	—	-0.14	—	1.12
–	M20	1	0.53	—	0.07	—	-0.38	—	0.07	—	0.66
–	NGC3576	1	0.13	—	0.65	—	-0.87	—	0.44	—	0.76
–	ORION 1	1	0.01	—	0.59	—	-1.38	—	0.02	—	0.85
–	ORION 2	1	0.00	—	0.67	—	-1.32	—	0.25	—	0.63
–	S209	19	0.08	0.03	0.61	0.01	-0.82	0.06	-0.52	0.08	3.08
–	S283	19	0.60	0.05	-0.33	0.05	-0.11	0.05	-0.52	0.08	1.44
–	S98	19	0.57	0.05	-0.26	0.13	-0.31	0.06	-0.48	0.09	2.35
–	S127	19	0.40	0.05	0.22	0.03	-0.76	0.04	-0.23	0.07	2.37
–	S128	19	0.32	0.05	0.59	0.01	-0.72	0.05	-0.20	0.08	2.25
IC10	# 2	4	0.16	0.05	0.85	0.05	-0.70	0.06	0.02	0.06	1.48
SMC	N80	1	0.54	—	0.53	—	-0.85	—	-0.37	—	-1.00
–	N83	1	0.36	—	0.63	—	-0.52	—	-0.29	—	0.12
–	N13	1	0.49	—	0.72	—	-1.01	—	-0.13	—	-1.00
–	N32	1	0.70	—	-0.54	—	-0.46	—	-0.50	—	0.15
–	N81	1	0.11	—	0.85	—	-0.93	—	-0.14	—	0.04
–	N66	1	-0.02	—	0.84	—	-0.97	—	-0.42	—	0.17
NGC295	1	21	0.44	0.04	0.45	0.09	-0.41	0.07	-0.32	0.15	0.50
–	2	21	0.56	0.03	0.52	0.09	-0.31	0.06	-0.42	0.16	0.57
–	3	21	0.52	0.04	0.61	0.10	-0.36	0.08	-0.21	0.18	0.60
–	6	21	0.24	0.04	0.72	0.08	-0.51	0.06	-0.07	0.16	0.43
–	7	21	0.59	0.05	0.23	0.12	-0.30	0.09	-0.35	0.16	0.54
–	8	21	0.40	0.04	0.31	0.10	-0.20	0.08	-0.14	0.14	0.39
–	9	21	0.29	0.09	0.77	0.14	-0.36	0.12	-0.14	0.18	0.40
M33	CC93	20	0.24	—	-0.80	—	-0.06	0.05	-0.27	0.03	0.20
–	IC142	20	0.36	0.01	0.01	0.01	-0.32	0.07	0.05	0.02	0.24
–	NGC595	20	0.33	0.01	0.28	0.01	-0.60	0.04	-0.01	0.01	0.49
–	NGC595	4	0.33	0.01	0.28	0.01	-0.51	0.05	0.01	0.05	0.49
–	MA 2	20	0.26	0.02	0.36	0.01	-0.71	0.02	0.01	0.02	0.10
–	NGC604	20	0.33	0.01	0.46	0.01	-0.43	0.04	-0.06	0.01	0.36
–	NGC604	4	0.33	0.02	0.46	0.01	-0.51	0.05	-0.17	0.05	0.36
–	NGC588	20	0.17	0.02	0.80	0.01	-0.72	0.11	-0.03	0.02	0.15
–	NGC588	4	0.17	0.02	0.80	0.01	-0.64	0.05	-0.01	0.07	0.15
–	IC131	4	0.32	0.01	0.72	0.01	-0.57	0.10	-0.06	0.08	0.10
NGC753	1	12	0.26	0.15	0.35	0.10	-0.20	0.15	-0.92	0.40	0.72
–	4	12	-0.15	0.15	0.35	0.10	-0.13	0.15	-0.68	0.30	0.18
–	17	12	-0.04	0.15	-0.53	0.10	-0.28	0.15	-0.42	0.30	0.85
–	20	12	0.00	0.15	0.29	0.10	-0.41	0.15	-0.88	0.30	0.35
–	23	12	0.06	0.15	0.40	0.10	-0.09	0.15	-1.00	0.30	0.99
Mkn 600	–	4	0.22	0.04	0.94	0.04	-0.73	0.09	-0.57	0.17	0.66
LMC	N59A	1	0.26	—	0.86	—	-0.87	—	-0.07	—	0.19
–	N44B	1	0.20	—	1.03	—	-0.74	—	0.02	—	0.09
–	N55A	1	0.33	—	0.56	—	-0.96	—	-0.01	—	0.10
–	N113D	1	0.68	—	0.50	—	-0.67	—	0.08	—	-1.00
–	N127A	1	0.65	—	0.49	—	-0.73	—	0.06	—	-1.00
–	N159A	1	0.11	—	0.79	—	-1.01	—	-0.02	—	0.43
–	N214C	1	0.52	—	0.59	—	-0.37	—	-0.05	—	0.00
–	N4A	1	0.13	—	0.75	—	-0.90	—	-0.03	—	0.25
–	N79E	1	0.43	—	0.24	—	-0.53	—	-0.15	—	0.16
–	N191A	1	0.86	—	—	—	-0.43	—	0.00	—	-1.00
IIZw40	–	4	-0.26	0.02	1.006	0.004	-0.83	0.06	-0.34	0.07	1.23
IIZw40	–	2	-0.26	0.02	1.006	0.004	-0.98	0.03	-0.23	0.03	1.23
NGC2366	NGC2363	4	-0.24	0.02	0.97	0.01	-1.06	0.06	-0.450	0.14	0.25
NGC2366	NGC2363 A1	8	0.30	0.08	0.72	0.08	-0.52	0.08	-0.39	0.21	0.19
–	NGC2363 A2	8	-0.36	0.01	1.00	0.01	-1.17	0.01	-0.50	0.02	0.20
–	NGC2363 A3	8	-0.10	0.18	0.91	0.07	-0.83	0.08	-0.29	0.22	0.18
–	NGC2363 A4	8	0.00	0.26	0.90	0.07	-0.60	0.11	-0.22	0.30	0.18

Table 1. Continued

Galaxy	**Region**	**Ref.**	**[OII]** 3727+ 3729	**Δ**	**[OIII]** 4959 + 5007	**Δ**	**[SII]** 6716+6731	**Δ**	**[SIII]** 9069+9532	**Δ**	**c(Hβ)**
NGC2403	VS35	5	0.39	0.06	0.26	0.04	-0.32	0.01	-0.10	0.03	1.06
–	VS24	5	0.38	0.04	0.24	0.04	-0.46	0.01	-0.04	0.04	-0.07
–	VS38	5	0.28	0.05	0.13	0.04	-0.52	0.01	-0.07	0.05	0.28
–	VS44	5	0.45	0.14	0.30	0.04	-0.41	0.01	-0.15	0.05	0.40
–	VS51	5	0.36	0.13	0.37	0.04	-0.47	0.01	-0.10	0.07	0.52
–	VS3	5	0.35	0.09	0.33	0.04	-0.49	0.01	-0.11	0.07	0.60
–	VS49	5	0.34	0.05	0.51	0.04	-0.39	0.01	-0.13	0.06	-0.10
NGC2541	6	21	0.35	0.09	0.66	0.19	-0.50	0.19	-1.15	0.36	0.38
–	16	21	0.28	0.07	0.74	0.09	-0.55	0.07	-0.21	0.16	0.44
–	17	21	0.40	0.04	0.63	0.09	-0.47	0.09	-0.38	0.15	0.36
–	19	21	0.48	0.04	0.46	0.09	-0.21	0.07	-0.21	0.16	0.42
UGC4483	–	18	-0.08	0.03	0.61	0.02	-0.93	0.01	-0.54	0.07	0.10
NGC2903	4	21	0.24	0.04	-0.01	0.09	-0.30	0.06	-0.21	0.14	0.28
–	5	21	0.00	0.05	-0.51	0.12	-0.26	0.07	-0.18	0.17	0.76
–	6	21	-0.36	0.08	-0.87	0.16	-0.41	0.07	-0.62	0.15	0.50
–	18	21	-0.20	0.08	-0.92	0.24	-0.27	0.12	-0.56	0.24	0.95
NGC2903	R1	15	-0.31	0.02	-0.76	0.03	-0.28	0.02	-0.56	0.10	0.82
–	R2	15	-0.37	0.03	-0.97	0.05	-0.28	0.02	-0.76	0.08	0.74
–	R3	15	-0.17	0.04	-0.41	0.04	-0.14	0.02	-0.16	0.13	0.46
–	R4	15	-0.24	0.04	-0.76	0.03	-0.23	0.02	-0.69	0.07	0.92
–	R6	15	-0.46	0.04	-1.03	0.06	-0.28	0.02	-0.69	0.07	0.79
–	R7	15	-0.41	0.03	-0.83	0.04	-0.24	0.01	-0.56	0.10	0.99
–	R8	15	-0.32	0.02	-0.76	0.03	-0.25	0.02	-0.69	0.07	0.96
IZw18	–	4	-0.59	0.06	0.46	0.01	-1.18	0.09	-0.85	0.18	0.04
IZw18	SE	17	-0.33	0.03	0.39	0.09	-1.15	0.34	-1.02	0.16	0.20
	NW	17	-0.59	0.02	0.44	0.09	-1.45	0.34	-1.09	0.16	0.10
NGC3310	Nuc	14	0.61	0.01	0.25	0.02	0.13	0.01	-0.01	0.01	0.63
–	A	14	0.41	0.01	0.48	0.01	-0.31	0.01	-0.37	0.01	0.29
–	B	14	0.49	0.01	0.38	0.01	-0.16	0.01	-0.22	0.01	0.20
–	C	14	0.50	0.01	0.51	0.01	-0.25	0.01	-0.09	0.01	0.34
–	E	14	0.50	0.01	0.44	0.01	-0.21	0.02	-0.12	0.01	0.26
–	L	14	0.67	0.01	0.36	0.02	-0.07	0.02	-0.17	0.02	0.53
–	M	14	0.40	0.01	0.53	0.03	-0.22	0.12	-0.11	0.10	0.14
NGC3351	R1	15	-0.37	0.03	-1.03	0.06	-0.35	0.02	-0.38	0.03	0.81
–	R2	15	-0.52	0.04	-0.92	0.05	-0.33	0.02	-0.56	0.10	0.24
–	R3	15	-0.52	0.03	-1.10	0.07	-0.37	0.03	-0.56	0.06	0.64
–	R4	15	-0.60	0.05	-1.18	0.08	-0.35	0.04	-0.35	0.06	0.24
–	R5	15	-0.26	0.03	-0.53	0.04	-0.21	0.04	-0.42	0.04	0.35
–	R7	15	-0.60	0.11	-1.10	0.07	-0.41	0.07	-0.76	0.15	0.28
–	R8	15	-0.60	0.06	-1.03	0.06	-0.37	0.05	-0.86	0.18	0.36
Mkn 36	–	4	0.10	0.04	0.85	0.04	-0.60	0.06	-0.54	0.17	0.12
NGC3504	R2	15	-0.15	0.02	-0.80	0.03	-0.18	0.03	-0.29	0.03	0.28
–	R3	15	-0.12	0.02	-0.62	0.02	-0.19	0.02	-0.35	0.03	0.59
–	R4	15	-0.15	0.04	-0.55	0.02	-0.12	0.03	-0.38	0.03	0.49
NGC3521	5	21	0.07	0.09	-0.96	0.16	-0.37	0.13	-0.69	0.30	0.98
–	7	21	0.41	0.05	-0.46	0.20	-0.20	0.12	0.08	0.23	1.24
–	8	21	0.61	0.05	0.62	0.12	-0.35	0.12	0.00	0.20	0.93
–	9	21	0.54	0.07	0.17	0.16	-0.23	0.14	0.24	0.22	0.75
NGC3621	1	21	0.32	0.03	-0.02	0.08	-0.23	0.05	-0.51	0.16	0.31
–	2	21	0.22	0.06	-0.10	0.11	-0.27	0.08	-0.69	0.18	0.13
–	3	21	0.50	0.04	0.24	0.10	-0.26	0.07	-1.16	0.18	0.84
NGC4253	A	6	0.20	0.07	0.71	0.03	-0.08	0.04	-0.03	0.06	0.51
–	B	6	0.43	0.05	0.65	0.03	-0.10	0.03	-0.05	0.06	0.45
NGC4254	142	10	-0.49	0.10	-0.97	0.14	-0.55	0.03	-0.46	0.04	0.77
–	78	10	-0.06	0.06	-1.27	0.30	-0.40	0.03	-0.51	0.05	0.82
–	173	10	-0.20	0.05	-1.03	0.10	-0.46	0.02	-0.42	0.04	0.38
–	185	10	0.16	0.09	-0.32	0.05	-0.32	0.02	-0.62	0.06	1.20
–	184	10	0.28	0.05	0.06	0.02	-0.19	0.03	-0.42	0.04	0.32
–	84	10	0.49	0.05	-0.19	0.05	-0.19	0.04	-0.12	0.06	0.58
–	22	10	0.51	0.03	0.03	0.02	-0.22	0.02	-0.12	0.03	0.59

Table 1. Continued

Galaxy	**Region**	**Ref.**	**[OII]** 3727+ 3729	Δ	**[OIII]** 4959 + 5007	Δ	**[SII]** 6716+6731	Δ	**[SIII]** 9069+9532	Δ	**c(Hβ)**
–	12	10	0.52	0.06	-0.25	0.07	-0.12	0.05	-0.08	0.07	0.29
NGC4303	95	11	0.09	0.12	-0.76	0.19	-0.29	0.11	-0.29	0.22	0.32
–	115	11	0.19	0.03	-0.80	0.15	-0.28	0.06	-0.69	0.18	0.78
–	155	11	0.11	0.04	-0.70	0.05	-0.32	0.05	-0.46	0.08	0.43
–	51	11	0.45	0.12	-0.51	0.18	-0.28	0.09	-0.76	0.20	0.74
–	76	11	0.40	0.08	-0.22	0.06	-0.29	0.09	-0.51	0.16	0.52
–	53	11	0.26	0.12	-0.48	0.25	-0.12	0.22	-0.69	0.18	0.38
–	103	11	0.24	0.13	-0.60	0.13	-0.26	0.12	-0.51	0.19	0.55
–	124	11	0.50	0.17	-0.48	0.17	-0.12	0.11	-0.42	0.13	0.48
–	148	11	0.48	0.08	-0.12	0.08	-0.19	0.08	-0.56	0.21	0.20
–	278	11	0.46	0.05	0.42	0.05	-0.21	0.08	-0.69	0.15	0.13
–	234	11	0.65	0.06	0.55	0.06	0.02	0.07	-0.12	0.21	0.00
NGC4528	4	21	0.29	0.03	0.16	0.07	-0.62	0.05	0.12	0.18	0.37
NGC4559	1	21	0.43	0.04	0.02	0.11	-0.13	0.09	-0.14	0.15	0.46
–	3	21	0.43	0.04	0.52	0.10	-0.32	0.07	-0.10	0.14	0.17
–	4	21	0.39	0.04	0.60	0.09	-0.58	0.08	-0.86	0.18	0.17
–	17	21	0.41	0.04	0.38	0.09	-0.28	0.07	0.12	0.16	0.49
–	18	21	0.48	0.03	0.35	0.07	-0.43	0.06	0.07	0.15	0.31
–	19	21	0.47	0.03	0.05	0.11	-0.28	0.08	0.01	0.17	0.45
–	20	21	0.43	0.04	0.00	0.10	-0.35	0.08	0.04	0.16	0.53
NGC4861	–	4	0.11	0.04	0.92	0.04	-0.75	0.06	-0.32	0.07	0.09
M51	CCM72	3	-0.21	0.02	-1.18	0.15	-0.43	0.04	-0.29	0.06	0.31
–	CCM24	3	0.01	0.01	-0.65	0.20	-0.38	0.03	-0.48	0.15	0.60
–	CCM10	3	0.21	0.01	-0.58	0.04	-0.40	0.06	-0.48	0.04	0.30
M101	H602	13	-0.59	0.03	-0.96	0.10	-0.47	0.04	-0.68	0.12	0.39
–	H493	13	0.05	0.11	-0.89	0.09	-0.32	0.03	-0.37	0.09	0.50
–	H507	13	-0.19	0.03	-1.00	0.04	-0.31	0.02	-0.41	0.09	0.46
–	H972	13	0.14	0.02	-0.40	0.03	-0.47	0.03	-0.14	0.08	0.30
–	H942	13	0.17	0.04	-0.41	0.07	-0.25	0.04	-0.30	0.10	0.52
–	H974	13	0.21	0.03	-0.47	0.10	-0.34	0.05	-0.66	0.16	0.33
–	H959	13	0.48	0.09	-0.42	0.05	-0.21	0.02	-0.28	0.09	0.52
–	H1013	13	0.26	0.02	0.12	0.02	-0.64	0.02	0.06	0.08	0.30
–	H399	13	0.19	0.05	-0.18	0.03	-0.46	0.02	-0.03	0.08	0.32
–	H1044	13	0.28	0.03	-0.12	0.03	-0.44	0.02	-0.06	0.08	0.28
–	H953	13	0.27	0.06	-0.25	0.04	-0.37	0.02	-0.33	0.08	0.24
–	H949	13	0.23	0.05	-0.43	0.03	-0.30	0.02	-0.17	0.08	0.39
–	H1052	13	0.32	0.04	0.50	0.02	-0.64	0.02	0.12	0.08	0.29
–	H203	13	0.36	0.02	-0.27	0.02	-0.26	0.02	-0.17	0.08	0.22
–	H1086	13	0.43	0.05	0.37	0.03	-0.46	0.01	-0.09	0.08	0.32
–	H875	13	0.53	0.05	0.09	0.03	-0.29	0.03	-0.21	0.08	0.43
–	H1098	13	0.49	0.04	0.18	0.02	-0.40	0.02	0.04	0.08	0.74
–	H237	13	0.11	0.02	0.19	0.02	-0.49	0.03	-0.25	0.08	0.20
–	H1026	13	0.37	0.02	0.57	0.02	-0.57	0.02	-0.07	0.08	0.11
–	H178	13	0.65	0.04	0.26	0.04	-0.43	0.02	-0.14	0.08	0.59
–	H1159	13	0.40	0.03	0.61	0.02	-0.64	0.02	-0.04	0.08	0.25
–	H1170	13	0.38	0.02	0.63	0.02	-0.54	0.03	-0.03	0.08	0.39
–	H1176	13	0.32	0.02	0.62	0.02	-0.70	0.02	0.00	0.08	0.39
–	H140	13	0.45	0.02	0.20	0.02	-0.11	0.02	-0.19	0.08	0.13
–	H1191	13	0.34	0.03	0.67	0.03	-0.60	0.03	-0.13	0.09	0.35
–	H119	13	0.49	0.09	0.35	0.03	-0.12	0.03	-0.52	0.10	0.33
–	H132	13	0.48	0.02	0.46	0.02	-0.34	0.02	-0.48	0.08	0.28
–	H143	13	0.45	0.02	0.54	0.02	-0.36	0.02	-0.08	0.08	0.39
–	H149	13	0.45	0.02	-0.39	0.02	-0.42	0.01	-0.06	0.08	0.45
–	H128	13	0.26	0.02	0.72	0.02	-0.70	0.02	-0.01	0.08	0.27
–	H67	13	0.37	0.02	0.68	0.02	-0.68	0.04	-0.13	0.08	0.07
–	H1216	13	0.29	0.03	0.79	0.02	-0.85	0.03	-0.07	0.08	0.17
–	H681	13	0.39	0.03	0.61	0.03	-0.57	0.05	-0.44	0.10	0.22
–	NGC5471	16	0.06	0.04	0.89	0.04	-0.61	0.05	-0.20	0.05	0.18
–	NGC5471	4	0.12	0.01	0.96	0.01	-0.70	0.05	-0.32	0.07	0.15
–	NGC5471A	13	0.11	0.03	0.97	0.02	-0.82	0.03	-0.30	0.08	0.22

Table 1. Continued

Galaxy	Region	Ref.	[OII] 3727+ 3729	Δ	[OIII] 4959 + 5007	Δ	[SII] 6716+6731	Δ	[SIII] 9069+9532	Δ	c(Hβ)
–	NGC5471A	2	0.17	0.03	0.81	0.02	-0.73	0.03	-0.35	0.03	0.25
–	NGC5471B	13	0.45	0.03	0.75	0.02	-0.27	0.02	-0.30	0.08	0.23
–	NGC5471C	13	0.36	0.03	0.80	0.02	-0.60	0.02	-0.20	0.08	0.19
–	NGC5471D	13	0.18	0.03	0.91	0.02	-0.80	0.03	-0.13	0.08	0.09
–	NGC5471E	13	0.10	0.03	0.91	0.02	-0.92	0.04	-0.14	0.08	0.24
–	S5	13	0.28	0.02	-0.48	0.03	-0.29	0.02	-0.10	0.08	0.30
–	S5	16	0.26	0.05	-0.49	0.06	-0.19	0.05	0.07	0.10	0.22
–	S5	2	0.32	0.04	-0.47	0.03	-0.17	0.05	0.30	0.07	0.50
–	NGC5455	13	0.32	0.02	0.68	0.02	-0.52	0.01	-0.08	0.08	0.12
–	NGC5455	16	0.41	0.04	0.68	0.04	-0.43	0.05	0.00	0.05	0.15
–	NCG5461	13	0.22	0.02	0.64	0.02	-0.68	0.02	0.08	0.08	0.36
–	NGC5461A	2	0.27	0.02	0.64	0.02	-0.47	0.02	0.00	0.01	0.60
NGC5953	A	7	-0.10	0.10	-0.52	0.04	-0.20	0.02	-0.46	0.04	0.00
–	B	7	-0.05	0.09	-0.44	0.06	-0.19	0.03	-0.49	0.05	0.00
–	C	7	0.20	0.07	0.36	0.02	-0.02	0.02	-0.44	0.03	0.00
IZw123	–	4	0.10	0.04	0.96	0.04	-0.64	0.06	-0.45	0.15	0.38
NGC7714	A	9	0.39	0.01	0.25	0.01	-0.13	0.01	-0.21	0.02	0.33
–	N110	9	0.26	0.02	0.27	0.01	-0.24	0.03	-0.02	0.05	0.30
–	B	9	0.38	0.01	0.68	0.01	-0.28	0.02	-0.31	0.02	0.37
–	C	9	0.45	0.04	0.54	0.01	-0.24	0.05	-0.38	0.09	0.44
–	N216	9	0.24	0.02	0.31	0.01	-0.23	0.03	0.03	0.05	0.30

References to the table

1: Dennefeld & Stasińska (1983); 2: Díaz *et al.* (1990);
3: Díaz *et al.* (1991); 4: Garnett (1989); 5: Garnett *et al.* (1997); 6: González-Delgado & Pérez (1996a); 7: González-Delgado & Pérez, (1996b); 8: González-Delgado *et al.* (1994);
9: González-Delgado
et al. (1995); 10: Henry *et al.* (1992); 11: Henry *et al.*
(1994); 12: Henry *et al.* (1996);
13: Kennicutt & Garnett (1996); 14: Pastoriza *et al.*
(1993); 15: Pérez-Olea (1996); 16: Shields & Searle (1978);
17: Skillman & Kennicutt (1993);
18: Skillman *et al.* (1993); 19: Vílchez & Esteban (1996);
20: Vílchez *et al.* (1988); 21: Zaritsky, Kennicutt & Huchra (1994).

terisk for which a measurement of the [OII] λ 7327 line has been used. The total oxygen abundance has been calculated as $log\frac{O}{H} = log\left(\frac{O^+}{H^+} + \frac{O^{++}}{H^+}\right)$. The errors in the abundances have been derived from those quoted for the emission lines whenever possible. For the HII regions in the Magellanic Clouds (Dennefeld & Stasińska 1983) we have adopted an abundance error of $\pm$ 0.10.

The oxygen abundance ranges from 2% solar for IZw18 to 70 % solar for region VS24 in NGC 2403.

We have included in the table data for three regions of metallicity close to solar for which detailed modelling has been made: CC93 in M33 (Vílchez *et al.* 1988), S5 in M101 (Shields & Searle 1978; Díaz *et al.* 1990) and the nucleus of NGC 3310 (Pastoriza *et al.* 1993).

3 RESULTS AND DISCUSSION

From the line intensities of the sulphur lines presented in Table 1 we have calculated the *sulphur abundance parameter* S_{23} defined as

$$S_{23} = \frac{[SII]\lambda\lambda 6717, 6731 + [SIII]\lambda\lambda 9069, 9532}{H\beta}$$

This parameter is analogous to the R_{23} parameter defined for the optical oxygen lines and hereafter we will refer to the oxygen and sulphur abundance parameters as O_{23} and S_{23} respectively. Both parameters are listed in Table 2.

The relation between O_{23} and the oxygen abundance for the objects in Table 2 can be seen in the upper panel of Fig 1 (solid dots) together with similar data for HII galaxies compiled by Díaz (1999) (open circles). The figure illustrates the problems mentioned in the introduction, the most important one being the two-valued nature of the relation which makes an accurate metallicity calibration virtually impossible, more so for objects with $logO_{23} \geq 0.8$. Also notice the position of the nucleus of NGC 3310 which is probably due to its higher than usual density ($n_H = 8000$ cm^{-3}; Pastoriza et al. 1993). On the contrary, and as expected, the relation between S_{23} and oxygen abundance for the objects of Table 2, shown in the lower panel of the figure, remains single valued up to a metallicity close to solar. In both figures the data corresponding to different observations of IZw18, NGC 5471 in M101, and S5 in M101 have been joined together to show the importance of internal errors. The solar metallicity regions have also been labelled.

Also, as compared to the case of O_{23}, the scatter in the relation between S_{23} and oxygen abundance is somewhat reduced.

The dependence of O_{23} on the degree of ionization of the nebula is partially responsible for the large scatter found in the O_{23} *vs* metallicity relation . Figure 2 (upper panel)

Table 2. Oxygen abundance and abundance parameters for the sample objects

Galaxy	Region	Ref	$logO_{23}$	$logS_{23}$	$12+log(O/H)$	$t_e(10^4K)$
MWG	N2467	1	0.75 ± 0.04	-0.03	8.01 ± 0.10	1.18
–	ETACAR	1	0.66 ± 0.04	0.18	8.37± 0.10	0.89
–	M17	1	0.75 ± 0.04	0.22	8.43± 0.10	0.88
–	M16	1	0.55 ± 0.04	-0.02	8.55± 0.10	1.81
–	M20	1	0.66 ± 0.04	0.20	8.50± 0.10	2.73
–	NGC3576	1	0.76 ± 0.04	0.46	8.42± 0.10	0.91
–	Orion1	1	0.69 ± 0.04	0.04	8.54± 0.10	0.84
–	Orion2	1	0.76 ± 0.04	0.26	8.50± 0.10	0.87
–	S127 *	19	0.62 ± 0.04	-0.12 ± 0.06	8.06± 0.26	0.80
–	S128 *	19	0.78 ± 0.02	-0.09 ± 0.06	8.04± 0.24	0.90
IC10	# 2	4	0.93 ± 0.01	0.09 ± 0.06	8.26 ± 0.10	1.08
SMC	N80	1	0.84 ± 0.04	-0.25	7.85± 0.10	1.39
–	N83	1	0.82 ± 0.04	-0.09	8.01± 0.10	1.21
–	N13	1	0.92 ± 0.04	-0.08	8.02 ± 0.10	1.30
–	N32	1	0.72 ± 0.04	-0.18	8.16± 0.10	2.13
–	N81	1	0.92 ± 0.04	-0.07	8.05 ± 0.10	1.26
–	N66	1	0.90 ± 0.04	-0.31	7.96 ± 0.10	1.31
M33	N604	4	0.70 ± 0.01	0.04 ± 0.02	8.51± 0.03	0.82
–	N604	20	0.70 ± 0.01	0.00 ± 0.02	8.51± 0.03	0.77
–	N595	4	0.61 ± 0.01	0.09 ± 0.02	8.44± 0.09	0.90
–	N595	20	0.61 ± 0.01	0.04 ± 0.02	8.44± 0.09	0.80
–	N588	4	0.89 ± 0.01	0.09 ± 0.03	8.33 ± 0.06	0.94
–	N588	20	0.89 ± 0.01	0.03 ± 0.03	8.33 ± 0.06	1.01
–	MA2	20	0.61 ± 0.01	0.09 ± 0.02	8.44 ± 0.15	0.80
–	IC142	20	0.52 ± 0.01	0.19 ± 0.03	8.69± 0.16	0.69
–	IC131	4	0.87 ± 0.01	0.06 ± 0.08	8.41 ± 0.06	0.95
–	CC93	20	0.28 ± 0.15	0.28 ± 0.04	9.02 ± 0.16	0.55
Mkn600	–	4	1.02 ± 0.04	-0.34 ± 0.12	7.86± 0.10	1.64
LMC	N59A	1	0.96 ± 0.04	-0.01	8.40± 0.10	1.01
–	N44B	1	1.09 ± 0.04	0.09	8.39± 0.10	1.11
–	N55A	1	0.76 ± 0.04	0.04	8.27± 0.10	0.98
–	N113D	1	0.90 ± 0.04	0.15	8.68± 0.10	0.87
–	N127A	1	0.88 ± 0.04	0.13	8.50 ± 0.10	0.95
–	N159A	1	0.87 ± 0.04	0.02	8.23± 0.10	1.07
–	N214C	1	0.86 ± 0.04	0.12	8.29± 0.10	1.04
–	N4A	1	0.84 ± 0.04	0.02	8.43± 0.10	0.93
–	N79E	1	0.65 ± 0.04	0.00	8.31± 0.10	0.92
–	N191A	1	0.92 ± 0.04	0.14	8.53± 0.10	1.09
IIZw40	–	4	1.04 ± 0.04	-0.22 ± 0.07	8.10± 0.10	1.33
IIZw40	–	2	1.01 ± 0.04	-0.15 ± 0.07	8.14± 0.02	1.28
N2366	N2363	4	1.00 ± 0.02	-0.39 ± 0.12	7.92± 0.04	1.48
–	N2363 A1	8	0.86 ± 0.08	-0.15 ± 0.15	7.74± 0.02	1.62
–	N2363 A2	8	1.02 ± 0.01	-0.42 ± 0.02	7.87± 0.02	1.61
–	N2363 A3	8	0.95 ± 0.08	-0.18 ± 0.20	7.82± 0.02	1.59
N2403	VS35	5	0.63 ± 0.05	0.10 ± 0.02	8.41± 0.14	0.84
–	VS24	5	0.62 ± 0.04	0.10 ± 0.03	8.76 ± 0.09	0.68
–	VS38	5	0.51 ± 0.05	0.06 ± 0.04	8.47± 0.10	0.76
–	VS44	5	0.68 ± 0.10	0.04 ± 0.04	8.49± 0.13	0.87
–	VS51	5	0.67 ± 0.08	0.05 ± 0.05	8.53± 0.15	0.80
–	VS3	5	0.64 ± 0.07	0.04 ± 0.05	8.41± 0.09	0.87
–	VS49	5	0.73 ± 0.04	0.06 ± 0.04	8.20± 0.08	1.05
UGC4483	–	18	0.69 ± 0.02	-0.39 ± 0.05	7.51± 0.04	1.66
IZw18	–	4	0.47 ± 0.01	-0.67 ± 0.15	7.27± 0.10	1.80
IZw18	SE	17	0.47 ± 0.01	-0.78 ± 0.08	7.27± 0.08	1.72
–	NW	17	0.48 ± 0.02	-0.93 ± 0.09	7.17± 0.06	1.96
N3310	Nuc	14	0.77 ± 0.01	0.37 ± 0.01	9.01± 0.15	0.62
–	A	14	0.75 ± 0.01	-0.04 ± 0.01	8.20 ± 0.10	1.04
–	B	14	0.74 ± 0.01	0.11 ± 0.01	8.13± 0.09	1.21
–	C	14	0.81 ± 0.01	0.14 ± 0.01	8.25± 0.04	0.95

Table 2. Continued

Object	Region	Ref.	$logO_{23}$	$logS_{23}$	$12+log(O/H)$	$t_e(10^4K)$
–	E	14	0.77 ± 0.01	0.14 ± 0.01	8.17± 0.08	0.98
–	L	14	0.84 ± 0.01	0.18 ± 0.02	8.47± 0.13	0.70
–	M	14	0.77 ± 0.02	0.14 ± 0.11	8.30± 0.15	0.97
Mkn36	–	4	0.92 ± 0.04	-0.27 ± 0.12	7.86 ± 0.10	1.50
N4861	–	4	1.10 ± 0.02	-0.18 ± 0.07	8.26± 0.10	1.21
M101	N5455	16	0.87 ± 0.04	0.14 ± 0.05	8.54 ± 0.10	0.89
–	N5471	16	0.95 ± 0.04	-0.06 ± 0.05	8.13 ± 0.10	1.19
–	N5471	2	1.00 ± 0.04	-0.20 ± 0.05	8.01± 0.10	1.28
–	N5471	4	1.00 ± 0.04	-0.16 ± 0.05	8.13± 0.05	1.30
–	N5461	2	0.79 ± 0.04	0.13 ± 0.05	8.46 ± 0.08	0.90
–	S5	2	0.38 ± 0.05	0.48 ± 0.08	8.90± 0.15	0.65
–	S5	16	0.33 ± 0.06	0.26 ± 0.08	9.10 ± 0.20	0.58
IZw123	–	4	1.02 ± 0.02	-0.23 ± 0.12	8.01± 0.10	1.41
N7714	A	9	0.62 ± 0.01	0.13 ± 0.01	8.47± 0.16	1.26
–	B	9	0.86 ± 0.01	0.01 ± 0.02	8.20 ± 0.09	1.11
–	C	9	0.80 ± 0.02	0.00 ± 0.07	8.27 ± 0.19	1.02
–	N110	9	0.57 ± 0.01	0.18 ± 0.04	8.53 ± 0.13	1.10
–	N216	9	0.58 ± 0.01	0.22 ± 0.04	8.46± 0.12	1.01

References to the table

1: Dennefeld & Stasińska (1983); 2: Díaz *et al.* (1990);
3: Díaz *et al.* (1991); 4: Garnett (1989); 5: Garnett *et al.* (1997); 6: González-Delgado & Pérez (1996a); 7: González-Delgado & Pérez, (1996b); 8: González-Delgado *et al.* (1994);
9: González-Delgado
et al. (1995); 10: Henry *et al.* (1992); 11: Henry *et al.*
(1994); 12: Henry *et al.* (1996);
13: Kennicutt & Garnett (1996); 14: Pastoriza *et al.*
(1993); 15: Pérez-Olea (1996); 16: Shields & Searle (1978);
17: Skillman & Kennicutt (1993);
18: Skillman *et al.* (1993); 19: Vílchez & Esteban (1996);
20: Vílchez *et al.* (1988); 21: Zaritsky, Kennicutt & Huchra (1994).

shows the relation between $logO_{23}$ and $log([OII]/[OIII])$, which can be taken as a good ionization parameter indicator for ionizing temperatures larger than about 35000 K (see Díaz 1999), for the objects in Table 1. A positive correlation between ionization parameter and O_{23} is evident for objects with O_{23} between 0.2 and 1 (higher excitation objects are at the left in the plot). On the contrary, no relation between $logS_{23}$ and $log([OII]/[OIII])$ is readily apparent in the lower panel of the figure. The peculiar position of IZw18 in the plots is due to its very low metallicity.

Based on the above considerations, we have attempted a calibration of oxygen abundance through the sulphur abundance parameter S_{23}, using the data of Table 2 with the exclusion of the three objects for which no direct determinations of the electron temperature exist: S5 in M101, CC93 in M33 and the nucleus of NGC 3310. A linear fit to the data, taking into account the observational errors, give:

$$12 + log(O/H) = 1.53 logS_{23} + 8.27$$

with a correlation coefficient of 0.88 and a value of $\sigma = 0.15$.

The data points corresponding to IZw18 deviate slightly from linearity. This is due to the high excitation of this object which increases the fraction of S^{++} converted to S^{3+} thus decreasing S_{23}. A quadratical fit:

$$12 + log(O/H) = 0.24(logS_{23})^2 + 1.42 logS_{23} + 8.25$$

provides a better fit to these extremely low metallicity data. The two fits are shown in the upper panel of Figure 3 by a solid and a dashed line respectively. The corresponding residuals are shown in the lower panel as a function of the oxygen abundance. Solid dots correspond to the linear fit while open circles correspond to the quadratic one.

Figure 4 shows the relation between S_{23} and O_{23}. The largest value of S_{23} corresponds to one of the observations of region S5 in M101 ($S_{23} = 0.48$), and the solar metallicity objects have S_{23} between 0.28 and 0.48. On the other hand, the object with the lowest metallicity known, IZw18, has a value of $logO_{23}$= 0.47. These two facts taken together imply that objects with $logO_{23} \leq 0.47$ and $-0.5 < logS_{23} \leq 0.28$ will necessarily have oversolar abundances. These objects are 48 out of the 196 listed in Table 1 and therefore constitute about a quarter of the total sample. Most of them are circumnuclear star forming regions, HII regions in inner galactic discs and HII regions in Virgo cluster galaxies.

For $logO_{23} > 0.45$ it can be seen that for the lowest metallicity objects there is a positive correlation between O_{23} and S_{23}; NGC 5471, with $logO_{23} \simeq 1.00$ and $logS_{23} \simeq 0.10$, would lie at the end of this correlation. Then, there is a trend of increasing S_{23} with decreasing O_{23} which corresponds to the "upper metallicity branch" of the O_{23} abundance calibration. For values of $logO_{23}$ between 0.45 and 0.00, the relation between the two abundance parameters is rather flat. Finally, for values of $logO_{23} < 0.0$ a trend of decreasing S_{23} with decreasing O_{23} is apparent, indicating that, for the metallicities involved, the expected reversal of the S_{23} *vs* metallicity relation has already taken place.

The behaviour of the O_{23} and S_{23} parameters is related with the different energies involved in the two sets of

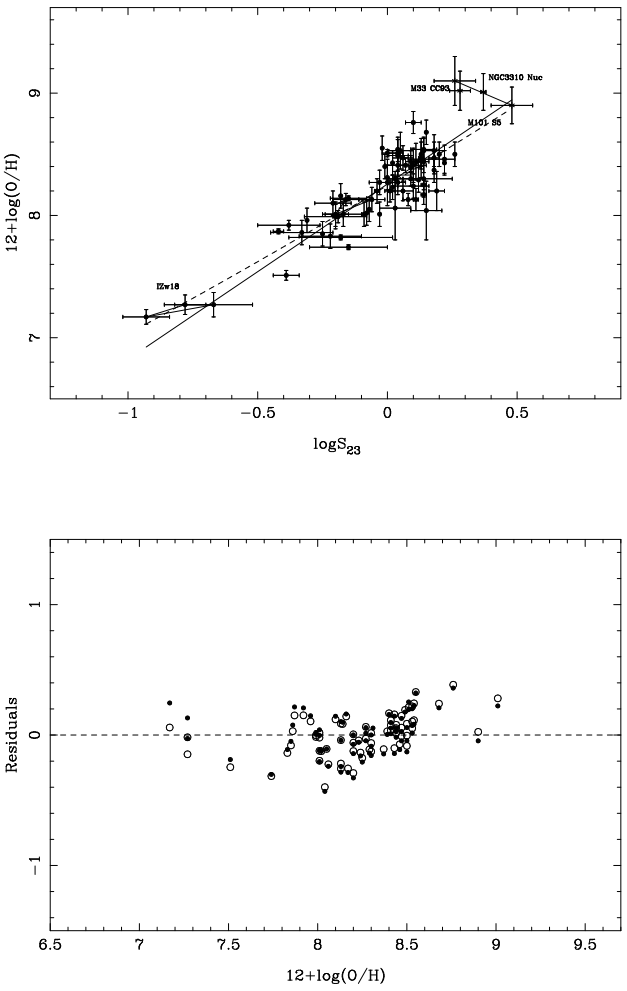

Figure 3. Empirical calibration of oxygen abundance through the sulphur abundance parameter S_{23}. The ressiduals of the fits are shown in the lower panel of the figure (see text for details).

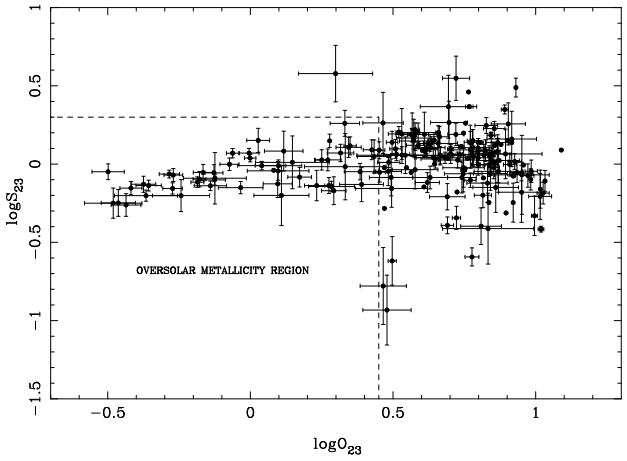

Figure 4. Relation between O_{23} and S_{23} for the objects in Table 1

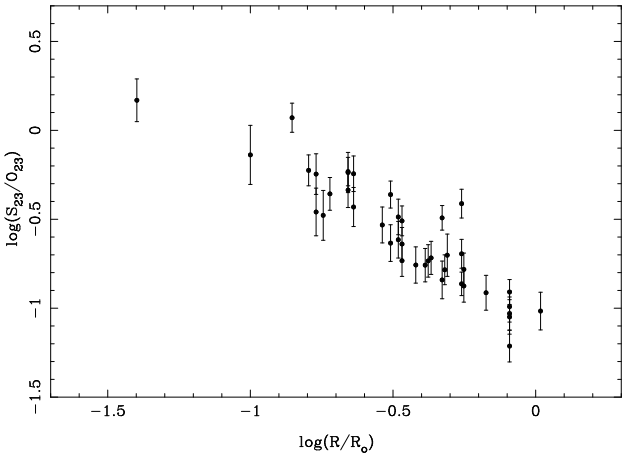

Figure 5. Variation of $log(S_{23}/O_{23})$ with galactic radius for M 101, which actally mimics a logarithmic abundance gradient through the disc.

transitions and therefore a combination of both should, in principle, be a better indicator of metallicity than either of them alone. Figure 5 shows a plot of $log(S_{23}/O_{23})$ for the HII regions in M 101 (Kennicutt & Garnett 1996). A single line logarithmic gradient is found. This might actually constitute a purely observational way to quantify galactic disc abundance gradients without the need to rely on theoretical photoionization models.

4 CONCLUSIONS

We have performed a new empirical calibration of nebular abundances using the sulphur abundance parameter S_{23}. This calibration is an alternative to the commonly used one based on the strong optical oxygen lines and presents several advantages. From the observational point of view, the lines are easily observable, both in low and high metallicity regions, and less affected by reddening. Furthermore, their intensities can be measured relative to nearby hydrogen recombination lines thus minimizing any effects due to uncertainties in flux calibration. On the theoretical side, their contribution to the cooling of the nebula becomes important at electron temperatures lower than in the case of the traditional O_{23} (previously called R_{23}) and therefore its relation with oxygen abundance remains single-valued up to metallicities close to solar. Also, the fact that S_{23} is less dependent than O_{23} on ionization parameter reduces the scatter in the relation.

The application of this new metallicity calibration can provide more accurate abundance determinations for objects with logO_{23} between 0.5 and 1.2, *i. e.* oxygen abundances between 12+log(O/H)= 7.20 ($\simeq$ 0.02 times solar) and 12+log(O/H) = 8.80 ($\simeq$ 0.75 times solar). This is the range of metallicities found in HII galaxies and HII regions in irregular galaxies and outer galactic discs.

Regarding HII regions of higher metallicity, the com-

posed parameter S_{23}/O_{23} can provide a better quantification of abundance gradients through galactic discs and might also hold the key to a future abundance calibration in this lower temperature regime.

ACKNOWLEDGEMENTS

This work has been partially supported by DGICYT project PB-96-052. We would like to thank Elena Terlevich and Bernard Pagel for a careful reading of the manuscript.

REFERENCES

Alloin, D, Collin-Souffrin, S, Joly, M. & Vigroux, L. 1979, *A&A*, 78, 200
Dennefeld, M. & Stasińska, G. 1983 *A & A* 118, 234
Díaz, A.I., Terlevich, E., Pagel, B.E.J., Vílchez, J.M. & Edmunds, M.G. 1990, *Rev. Mex. Astron. Astrof.* 21, 223
Díaz, A.I., Terlevich, E., Vílchez, J.M., Pagel, B.E.J. & Edmunds, M.G. 1991, *MNRAS* 253, 245
Díaz, A.I. 1999, in preparation.
Dopita, M.A. & Evans, I.N. 1986, ApJ, 307, 431
Edmunds, M.G. & Pagel, B.E.J. 1984, MNRAS, 211, 507
Garnett, D.R. 1989, *ApJ* 345, 282
Garnett, D.R., Shields, G.A., Skillman, E.D., Sagan, S.P. & Dufour, R.J. 1997, *ApJ* 489, 63
González-Delgado, R.M. & Pérez, E. 1996a, *MNRAS* 278, 737
González-Delgado, R.M. & Pérez, E. 1996b, *MNRAS* 281, 781
González-Delgado, R.M., Pérez, E., Tenorio-Tagle, G., Vílchez, J.M., Terlevich, E., Terlevich, R., Telles, E., Rodríguez-Espinosa, J.M., Mas-Hesse, M., García-Vargas, M.L., Díaz, A.I., Cepa, J. & Castañeda, H.O. 1994, *ApJ* 437, 239
González-Delgado, R.M., Pérez, E., Díaz, A.I., García-Vargas, M.L. Terlevich, E. & Vílchez, J.M. 1995, *ApJ* 439, 604
Henry, R.B.C., Pagel, B.E.J., Lasseter, D.F. & Chincarini, G.L. 1992, *MNRAS* 258, 321
Henry, R.B.C., Pagel, B.E.J. & Chincarini, G.L. 1994, *MNRAS* 266, 421
Henry, R.B.C., Balkowski, C., Cayatte, V., Edmunds, M.G. & Pagel, B.E.J. 1996, *MNRAS* 283, 635
Kennicutt, R.C. & Garnett, D.R. 1996, *ApJ*, 456, 504
McCall, L.M., Rybski, P.M & Shields, G.A. 1985, ApJS, 57, 1
McGaugh, S.S., 1991, ApJ, 380,140
Pagel, B.E.J., Edmunds, M.G., Blackwell, D.E., Chun, M.S. & Smith, G., 1979, MNRAS, 189, 95
Pastoriza, M.G., Dottori, H.A., Terlevich, E., Terlevich, R. & Díaz, A.I. 1993, *MNRAS* 260, 177
Pérez-Olea, D. 1996, *PhD Thesis, UAM*
Shields, G.A. & Searle, L. 1978, *ApJ* 222, 281
Skillman, E.D., 1989, ApJ, 347, 883
Skillman, E.D. & Kennicutt , R.C. 1993, *ApJ* 347, 875
Skillman, E.D., Terlevich, R.J., Kennicutt, R.C., Garnett, D.R. & Terlevich, E. 1993, *ApJ* 411, 655
Vílchez, J.M. & Esteban, C. 1996, *MNRAS* 280, 720
Vílchez, J.M., Pagel, B.E.J., Díaz, A.I., Terlevich, E. & Edmunds, M.G. 1988, *MNRAS* 235, 633
Zaritsky, D., Kennicutt, R.C. & Huchra, J.P. 1994, *ApJ* 420, 87